Regional and Teleconnected Impacts of Radiation-Topography Interaction over the Tibetan Plateau

Dalei Hao[1], Gautam Bisht[1], Yu Gu[2], and L. Ruby Leung[1]

[1]Atmospheric Sciences and Global Change Division, Pacific Northwest National Laboratory, Richland, WA, USA

[2]Joint Institute for Regional Earth System Science and Engineering and Department of Atmospheric and Oceanic Sciences, University of California, Los Angeles, CA, USA

Corresponding author: Dalei Hao (dalei.hao@pnnl.gov)

Key Points:

- Topography-radiation interaction over the Tibetan Plateau increases annual average near-surface air temperature of the region by 0.26 K.
- Radiation-topography interaction over the Tibetan Plateau also affects the precipitation patterns in South and East Asia.
- Including radiation-topography interaction overall improves the simulation of surface climate over the Tibetan Plateau and Asian regions.

Abstract

Radiation-topography interaction plays an important role in surface energy balance over the Tibetan Plateau (TP). However, the impacts of such interaction over the TP on climate locally and in the Asian regions remain unclear. This study uses the Energy Exascale Earth System Model (E3SM) to evaluate the regional and teleconnected impacts of radiation-topography interaction over the TP. Land-atmosphere coupled experiments show that topography regulates the surface energy balance, snow processes, and surface climate over the TP across seasons. Accounting for radiation-topography interaction overall improves E3SM's performance in simulating surface climate. The winter cold bias in air temperature decreases from -4.48 K to -3.70 K, and the wet bias in summer precipitation is mitigated in southern TP. The TP's radiation-topography interaction further reduces the South and East Asian summer precipitation biases. Our results demonstrate the topographic roles in regional climate over the TP and highlight its teleconnected climate impacts.

Plain Language Summary

The Tibetan Plateau (TP) is characterized by high elevation and complex topography. Interaction between solar radiation and the undulating topography has important impacts on the regional surface energy balance and hydrologic cycle. Here we use Earth System Model simulations to show the local and remote impacts of the TP's radiation-topography interaction on the surface climate of the Asian regions. Such interaction overall increases the air temperature especially in winter over the TP and reduces the summer precipitation in southern TP. Teleconnectedly, the interaction further alters the precipitation patterns in South and East Asia, by altering the atmospheric circulation that influences moisture transport and clouds. Accounting for such interaction generally improves the model performance when benchmarked against observations. These findings underscore the important roles of the TP's radiation-topography interaction in modulating the climate of the local and remote Asian regions.

1 Introduction

Radiation-topography interaction plays an important role in the surface energy balance [*Arnold et al.*, 2006; *Lee et al.*, 2019]. Compared to flat terrain, rugged terrain alters direct solar radiation, due to the local solar geometry, self-shadowing and cast shadowing from adjacent terrain [*Dubayah and Rich*, 1995; *Olson and Rupper*, 2019]. Besides direct solar radiation, the occlusion of adjacent terrain reduces diffuse radiation from sky [*Proy et al.*, 1989], while the reflected radiation from adjacent terrain increases the solar radiation received by the surface, due to the multi-scattering effects [*Sirguey*, 2009]. Neglecting the adjustment and redistribution of solar radiation over mountainous regions due to its interaction with topography can cause large uncertainties in modeling surface energy and water cycles [*Comola et al.*, 2015; *Liou et al.*, 2013], snow processes [*Hao et al.*, 2022], land-atmosphere interaction, and atmospheric circulation and clouds [*Cai et al.*, 2023; *Gu et al.*, 2022; *Lee et al.*, 2019].

Parameterizations of radiation-topography interaction have been recently developed and incorporated in a few Earth System Models (ESMs). However, nearly all the ESMs that participated in the Coupled Model Intercomparison Project Phase-6 (CMIP6) adopt a simple plane-parallel (PP) two-stream approximation scheme to describe the radiative transfer processes with the assumption of flat surface. Based on the Monte Carlo photon tracing simulations, Lee et al. (2011) developed a computationally-efficient radiative transfer parameterization (TOP) for rugged terrain to consider the subgrid topographic effects on solar radiation. This TOP parameterization has been recently implemented in the Community Earth System Model (CESM) [*Lee et al.*, 2019], Energy Exascale Earth System Model (E3SM) [*Hao et al.*, 2021], and Geophysical Fluid Dynamics Laboratory (GFDL) ESM [*Zorzetto et al.*, 2023]. Such model enhancement allows us to systematically explore the impacts of radiation-topography interaction regionally and globally.

Radiation-topography interaction has been found to have large impacts on land surface and atmospheric processes over mountainous regions such as the Tibetan Plateau (TP). Driven by meteorological forcing, offline land simulations have shown non-negligible effects of topography on shortwave radiation balance, surface turbulent heat flux, snow cover, and surface temperature across a wide range of spatial resolutions from 1-km to 2° [*Hao et al.*, 2021; *Hao et al.*, 2022; *Zhang et al.*, 2022; *Zorzetto et al.*, 2023]. However, offline land simulations neglect the impacts of land-atmosphere interaction, motivating the use of land-atmosphere coupled ESM experiments to investigate how radiation-topography interaction impacts both atmospheric and land processes over the TP. Most ESMs tend to underestimate air temperature (T_{air}) and overestimate precipitation (P) over the TP across seasons [*Cui et al.*, 2021; *Zhu and Yang*, 2020]. The inclusion of radiation-topography interaction in land-atmosphere coupled CESM simulations reduces the cold bias over the TP in winter [*Lee et al.*, 2019], and overall decreases P across seasons [*Fan et al.*, 2019].

Besides local impacts, changes in the elevated heating due to radiation-topography interaction over the TP may influence the climate in other regions through teleconnection by excitation of Rossby waves. As the highest plateau in the Earth surface with large snow cover, TP plays an important role in modulating the atmospheric circulation and shaping the weather and climate around the TP [*Wu et al.*, 2014; *Wu et al.*, 2007; *Yang et al.*, 2020]. For example, the spring surface temperature over the TP shows a lag correlation with summer P in East Asia [*Xue et al.*, 2022]. Xue et al. [2022] identified an out-of-phase oscillation between the TP and Rocky Mountain surface temperature and suggested that TP may provide a substantial source of subseasonal-to-seasonal predictability for P in many global regions. Changing snow cover over the TP can advance/delay the onset and strengthen/weaken the intensity of the East Asian Summer Monsoon, and strongly influence the South Asian Summer Monsoon precipitation [*Li et al.*, 2018; *You et al.*, 2020]. The projected surface darkening due to reduced snowpack by global warming will strengthen the elevated heat pump of the TP, and further impact the remote Asian monsoon systems [*Tang et al.*, 2023]. Likewise, the radiation-topography interaction-induced changes in land surface thermal conditions over the TP are expected to regulate the transport of water and heat to the Asian downstream regions and further impact the climate of these surrounding regions.

This study aims to investigate the regional and teleconnected impacts of radiation-topography interaction over the TP. Specifically, we used E3SM to carry out present-day 40-year land-atmosphere coupled experiments using three different model configurations to isolate the impact of radiation-topography interaction over the TP. Using these experiments and six benchmark datasets, we evaluated the local impacts of radiation-topography interaction on the TP's surface climate across seasons, followed by analysis of the remote impacts of the TP on T_{air} and P patterns of the East and South Asian regions.

2 Materials and Methods

2.1 Radiation-topography interaction in E3SM

E3SM, supported by the United States Department of Energy (DOE), is a state-of-the-art fully-coupled ESM developed to address the grand challenge of robust, actionable predictions of the variability and change of the Earth system [*Leung et al.*, 2020]. Rooted from CESM version-1, the latest version-2 of E3SM (E3SMv2) features significant developments especially in the atmospheric dynamical core and physics parameterization schemes, river routing, ocean and sea ice components [*Golaz et al.*, 2022]. Compared to its predecessor E3SM version-1, E3SMv2 shows a higher computational efficiency and improved performance in simulated clouds and P patterns [*Golaz et al.*, 2022]. The E3SM Land Model version-2 (ELMv2), which originated from the Community Land Model version-4.5, includes a more realistic snow albedo parameterization [*Dang et al.*, 2019] and an improved land biogeochemistry representation [*Burrows et al.*, 2020] for various simulation campaigns. The new optional radiation-related configurations in ELMv2 include the TOP parameterization [*Hao et al.*, 2021], support for multiple types of snow grain shape (i.e., spherical and non-spherical), and updates to the snow albedo parameterizations to account for different mixing states of snow grain and light-absorbing particles (LAP) [*Hao et al.*, 2023].

ELMv2, by default, uses the PP parameterization to calculate surface shortwave radiation balance without accounting for the impacts of topographic relief. The new TOP parameterization in ELMv2 can capture the subgrid topographic effects on solar radiation [*Hao et al.*, 2021]. TOP represents the relationship between the topography-related factors (i.e., the grid-average cosine of local solar incident angle, sky view factor, terrain configuration factor, and standard deviation of elevation) and the radiation adjustments caused by subgrid topography via multiple linear regression [*Hao et al.*, 2021; *Lee et al.*, 2011]. The land-only ELM simulations showed that TOP has better performance in simulating surface energy balance and water cycles in the TP than PP [*Hao et al.*, 2021; *Hao et al.*, 2022]. The performance of TOP in land-atmosphere coupled simulations in and around the TP is evaluated in this study.

2.2 Experimental Design

We conducted land-atmosphere coupled present-day simulations using E3SMv2 with three different configurations: 1) the default PP scheme, denoted as PP_Globe; 2) the TOP scheme for the TP region and PP for the rest of the globe (Figure S1), denoted as TOP_TP; and 3) the TOP scheme for the global land, denoted as TOP_Globe. For each simulation, we used the F2010 component set with only active land, atmosphere and river components. In the F2010 configuration, the solar constant, sea surface temperature, sea ice, greenhouse gas concentrations, and aerosol emissions are prescribed at the 2010 level. The E3SM Atmosphere Model version-2 (EAMv2) was set at approximately 1° spatial resolution with 72 vertical layers. ELMv2 was configured at a 0.5° spatial resolution in the satellite phenology mode driven by the satellitederived climatological leaf area index data. We ran 40-year global simulations and used the last 20-year simulations for model analysis. Both the EAMv2 and ELMv2 outputs were aggregated to seasonal and annual mean. The EAMv2 outputs were resampled to 0.5° for further analysis.

2.3 Model Analysis and Evaluation

To clarify the role of radiation-topography interaction, the three model simulations described in Section 2.2 were compared in the TP and downstream over East and South Asia, across the seasons: winter (DJF), spring (MAM), summer (JJA), autumn (SON) as well as annual average. Specifically, the difference between TOP_TP and PP_Globe was used to investigate the local and remote impacts of radiation-topography interaction over the TP. We also evaluated the difference between TOP_Globe and PP_Globe to diagnose the impacts of non-TP mountainous regions. Specifically, for the local impacts, we compared the spatiotemporal differences in land surface albedo (α), surface radiation fluxes, turbulent heat fluxes, snow cover fraction (f_{sno}), snow water equivalent (*SWE*), T_{air}, and P. For the remote effects, we investigate the impacts on T_{air} and P in two subregions: South Asia (SA; 10-25°N, 70-100°E) and East Asia (EA; 17-49°N, 105-140°E).

We collected six benchmark datasets from 2005-2015 for model evaluation (Table S1): (1) the surface radiation fluxes from the Clouds and the Earth's Radiant Energy System (CERES) Energy Balanced and Filled (EBAF) Edition 4.2 [*Nasa/Larc/Sd/Asdc*, 2023], (2) latent (F_{lat}) and sensible (F_{sen}) heat fluxes from FLUXCOM [*Jung et al.*, 2019], (3) the spatially- and temporally-complete (STC) snow-covered area and grain size (STC-MODSCAG) product [*Rittger et al.*, 2020], (4) the snow property inversion from remote sensing (SPIReS) product [*Bair et al.*, 2021]), (5) T_{air} from the University of Delaware (UDel) v5.01 terrestrial air temperature monthly data [*Willmott and Matsuura*, 1995], and (6) P from the Global Precipitation Climatology Project (GPCP) v2.3 [*Adler et al.*, 2018; *Huffman et al.*, 1997]. We used the average of STC-MODSCAG and SPIReS as the reference values of f_{sno}. All the datasets were resampled spatially to 0.5° and temporally to multi-year average seasonal mean to be identical with the model outputs. Based on these benchmark datasets, statistical metrics including correlation coefficient (R), area-weighted mean bias, and area-weighted root-mean-square-error (RMSE) were used to evaluate the model performance. We also calculated the relative difference (δ; unit: %) between the mean bias of TOP_TP ($\mathrm{Bias}_{\mathrm{TOP\_TP}}$) and that of PP_Globe ($\mathrm{Bias}_{\mathrm{PP\_Globe}}$) as $(|\mathrm{Bias}_{\mathrm{TOP\_TP}}| - |\mathrm{Bias}_{\mathrm{PP\_Globe}}|)/|\mathrm{Bias}_{\mathrm{PP\_Globe}}|*100$.

3 Results

3.1 Regional impacts on surface energy balance and surface climate

Radiation-topography interaction regulates the annual average surface energy balance over the TP. In TOP_TP, topography reduces α by 0.01 (mean value), especially in the central and southern TP by more than 0.05, while increasing α in the northern border of the TP (Figure 1a). TOP_TP shows lower cloud cover (Figure S2f) and thus larger downward solar radiation by 0.28 W/m^2 (mean value) than PP_Globe (Figure S2a). Consequently, TP absorbs more solar radiation with the mean value of about 2.10 W/m^2 (Figure 1b), driven by the reduction of α and increase of downward solar radiation. Given that TP has an annual average downward solar radiation of 231 W/m^2 and annual average α of 0.34 in PP_Globe, the α reduction induced by topography accounts for about 96% of the increase in net solar radiation (R^s_{net}), while the downward solar radiation changes only account for about 4% of the difference between TOP_PP and PP_Globe over the TP. The downward longwave radiation shows a small change of 0.19 W/m^2 in mean value (Figure S2b) responding to the cloud cover change, while the upward longwave radiation increases by 1.27 W/m^2 (mean value) (Figure S2c) associated with surface warming (Figure 1g). The change in radiation fluxes further increases both F_{lat} and F_{sen} (Figure 1c-d). F_{sen} shows a larger increase by 0.79 W/m^2 (mean value) than F_{lat} (0.18 W/m^2). For the seasonal variation, overall winter shows larger α reduction than summer (Figure S3a) due to higher snow cover and snow albedo. However, the topography-induced changes in R_{net}^s for all the four seasons are comparable (Figure S3b), because the seasonal variation of solar angle affects the available solar radiation. Although F_{sen} increases for all seasons (Figure S3d), F_{lat} shows smaller changes for all seasons and even decreases in autumn (Figure S3c). Besides the TP mean changes, the spatial patterns of the differences in radiative fluxes show larger seasonal variations (Figures S4-S7).

The increasing R_{net}^s overall decreases annual average f_{sno} over the TP (Figure 1e). The spatial pattern of the change in annual average f_{sno} is consistent with that of α (Figure 1a,e), attributed to the positive snow albedo feedback [*Thackeray and Fletcher*, 2016] where the darkened snow absorbs more solar radiation, accelerate snow aging and melt, and thus reduces f_{sno}, which further reduces α. Different from f_{sno}, SWE increases in the western TP and decreases in the central and southern TP (Figure 1f). Although topography can accelerate snow melt (Figure S2e), the increasing snowfall compensates the loss of snow masses over the western TP (Figure S2f). The snow-atmosphere interaction complicates the snow changes caused by topography compared to the offline land simulations. At the seasonal scale, similar to α, f_{sno} shows larger differences in cold seasons and the smallest changes in summer due to the smaller snow cover (Figure S3e). Similarly, SWE shows the largest decrease by 4.3 mm in winter (Figure S3f).

The increase in F_{sen} leads to higher annual average near-surface (i.e., 2 m) T_{air} over the whole TP (Figure 1g) by a mean value of 0.26 K. The increase in T_{air} for winter is more pronounced with a mean value of 0.78 K, while there is a slight decrease in the western and Southern TP for summer (Figures S3g and S6). The changing T_{air} and F_{lat} affect the water and heat exchange between land and atmosphere, and eventually affect the regional P. Overall the central and northern TP shows a decrease in annual average P, while the western TP shows an increase (Figure 1h). The seasonal differences in P are well correlated with the differences in clouds (Figure S2f). Topography reduces the summer P by 0.1 mm/day (mean value), especially in the central and southern TP (Figure 2h), related to the changing winds and cloud cover (Figures S2 and S8). The topography-induced increase in winter T_{air} and decrease in summer P are expected to reduce the cold and wet bias of E3SM in the TP.

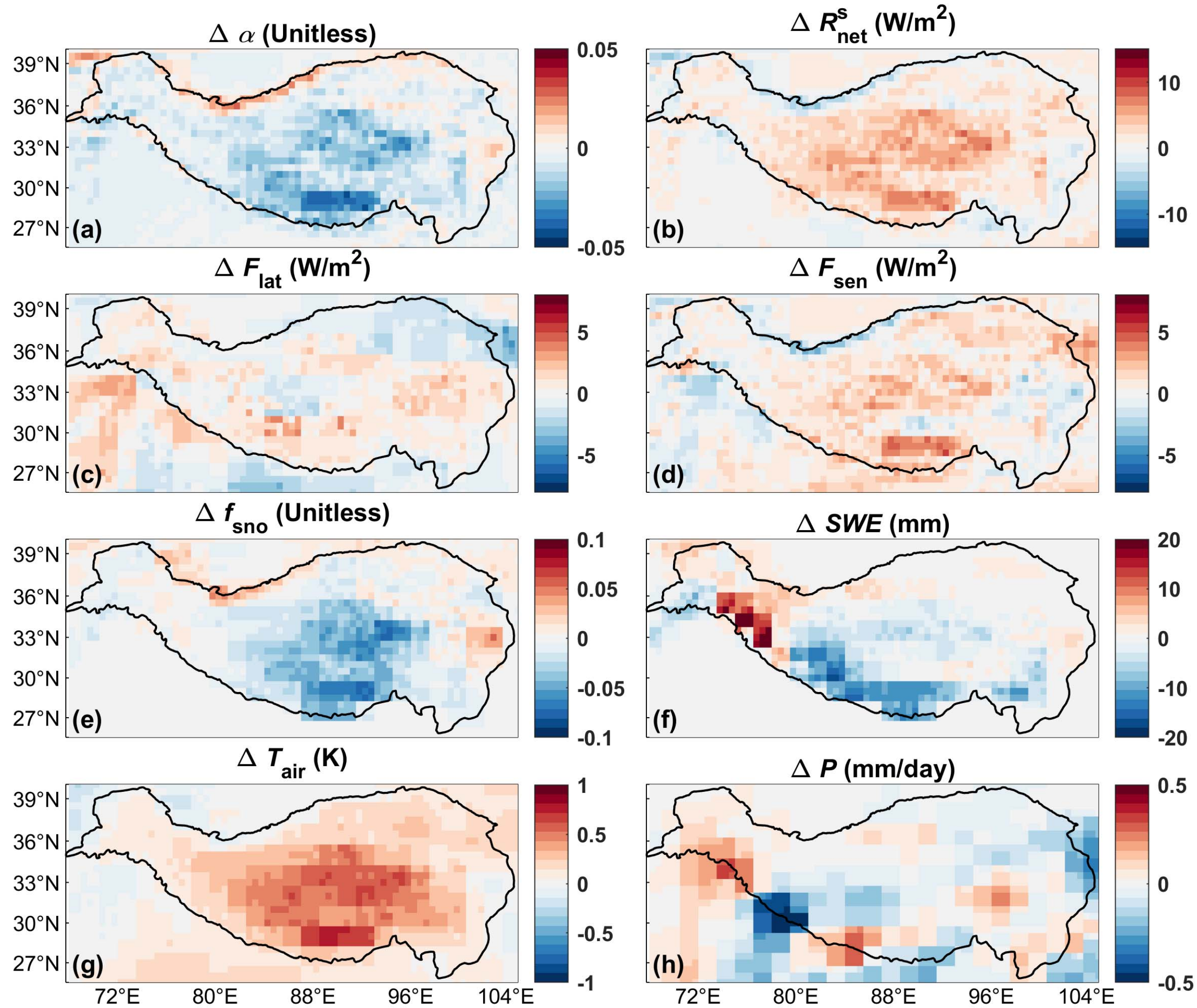

Figure 1. Regional impacts of radiation-topography interaction on annual (a-d) surface energy balance, (e-f) snow, (g) air temperature (T_{air}) and (h) precipitation (P) over the TP. For each panel, the impacts are represented by the difference (Δ) between TOP_TP and PP_Globe.

Including radiation-topography interaction overall improves the E3SM model performance in simulating surface energy balance, snow processes, and surface climate over the TP. For the annual scale, TOP_TP generally shows similar correlation, but smaller mean bias and RMSE with/than PP_Globe (Table 1). For example, δ of α is -7.4% which means that the mean bias of TOP_TP reduces 7.4% compared to that of PP_Globe, while the mean biases of R_{net}^{s}, f_{sno} and T_{air} reduces 23.2%, 6.7% and 11.1%, respectively. Seasonally (Table S2), for α, both TOP_TP and PP_Globe show high correlation (>=0.59) with CERES across seasons, but large positive mean bias and large RMSE, especially in winter. TOP_TP reduces about 5% and 6% of the mean biases compared to PP_Globe for winter and spring. For R_{net}^{s}, TOP_TP improves the correlation with CERES from 0.62 (PP_Globe) to 0.68 in winter and from 0.39 (PP_Globe) to 0.53 in autumn. TOP_TP shows slightly higher positive mean biases in summer, but lower negative mean biases and smaller RMSEs than PP_Globe in other seasons. For F_{lat}, both TOP_TP and

PP_Globe are similarly well correlated with FLUXCOM, but show large overestimations in non-winter seasons, although TOP_TP shows slightly lower negative mean biases in winter than PP_Globe. For F_{sen}, both TOP_TP and PP_Globe show low R values, high negative mean biases and large RMSEs especially in the warm seasons. Compared to PP_Globe, TOP_TP shows higher correlations in winter and autumn, and smaller negative mean biases across seasons than PP_Globe. F_{lat} and F_{sen} generally show opposite mean biases, implying that there are large uncertainties in partitioning the turbulent heat fluxes in E3SM. For f_{sno}, TOP_TP shows slightly better performance for all the three metrics. For T_{air}, TOP_TP shows similar R values with PP_Globe but reduces the cold bias especially in the cold seasons. For example, the negative mean bias of winter T_{air} deceases from -4.57 K to -3.79 K. For P, TOP_TP generally has similar mean biases and RMSEs, but higher R values than PP_Globe. For example, R increases from 0.65 to 0.72 in spring, and TOP_TP also slightly reduces the summer wet bias.

Comparing TOP_Globe and PP_Globe produces results that are spatially (Figure S9) and temporally (Figure S10) similar to the comparison between TOP_TP and PP_Globe, despite some differences in the magnitude of the statistical metrics. The corresponding evaluation results are shown in Table S3.

Table 1. Statistical metrics of E3SM simulated annual surface energy balance, snow variables, air temperature (T_{air}) and precipitation (P) against the benchmark datasets over the TP for both PP_Globe and TOP_TP. The sources of the benchmark datasets are indicated in the second column. The corresponding metrics across seasons are listed in Table S2.

Variable	Benchmark dataset	R_{PP_Globe}	R_{TOP_TP}	$Bias_{PP\_Globe}$	$Bias_{TOP\_TP}$	$RMSE_{PP\_Globe}$	$RMSE_{TOP\_TP}$	δ (%)
Land surface albedo (α, Unitless)	CERES-EBAF Edition 4.2	0.70	0.72	0.11	0.10	0.14	0.13	-7.4
Net solar radiation (R_{net}^{s}, W/m^2)	CERES-EBAF Edition 4.2	0.15	0.20	-9.03	-6.94	24.41	22.88	-23.2
Latent heat flux (F_{lat}, W/m^2)	FLUXCOM	0.81	0.81	15.69	15.98	17.36	17.58	1.9
Sensible heat flux (F_{sen}, W/m^2)	FLUXCOM	-0.10	-0.07	-19.60	-18.74	23.41	22.52	-4.4
Snow cover fraction (f_{sno})	STC-MODSCAG and SPIRES	0.37	0.40	0.22	0.20	0.28	0.27	-6.7
Air temperature (T_{air}, K)	UDel v5.01	0.56	0.57	-2.36	-2.10	5.69	5.50	-11.1
Precipitation (P, mm/day)	GPCP v2.3	0.80	0.81	1.46	1.44	1.88	1.86	-1.2

3.2 Teleconnected impacts on East and South Asian air temperature and precipitation

Including radiation-topography interaction over the TP overall reduces the bias of T_{air} in the land regions of SA and EA. PP_Globe and TOP_TP show similarly high correlations with the UDel data across seasons with R values ≥0.70 and ≥0.89, respectively in SA and EA (Table S4). PP_Globe shows cold biases in annual T_{air} over the TP's surrounding Asian regions (Figure 2a). For annual average in SA, PP_Globe has a cold bias of -1.28 K, while in EA, the cold bias is -0.90 K. For summer, PP_Globe has a cold bias of -0.89 K in SA, but a warm bias of +0.54 K in EA. Compared to PP_Globe, TOP_TP increases the annual and summer T_{air} in India, but shows small changes in other SA regions. The winter in SA shows larger reductions of T_{air} bias by 0.24 K than other seasons (Table S4). In EA, TOP_TP increases annual T_{air} in north China, but reduces annual T_{air} in other EA regions. For summer, TOP_TP reduces the warm biases in northeast Asia, but increase the biases in north China. The summer warm bias in EA reduces from +0.54 K of PP_Globe to +0.49 K of TOP_TP.

Radiation-topography interaction over the TP affects the *P* patterns in EA and SA, possibly through its influence on the atmospheric circulation. Overall the impacts of such interaction on annual and summer *P* show very heterogeneous spatial patterns in the Asian regions (Figure 2d,h). In India and East China, TOP_TP overall shows smaller annual average *P* than PP_Globe (Figure 2d). In summer, TOP_TP reduces *P* in India, but increases it in the eastern regions of SA (Figure 2h). This is because the topography-induced wind anomaly weakens the climatological westerly wind and associated water transport from the Arabian Sea, while intensifying water transport from the continent to the Bay of Bengal (Figure S8). The summer *P* difference between TOP_TP and PP_Globe shows a tripolar structure of "north decrease–middle increase–south decrease" in East China (Figure 2h), which is a dominant pattern of *P* natural variability of the region [*Xue et al.*, 2023]. The tripolar pattern of changes in P is associated with the pattern wind changes at 850-hPa which enhance convergence of water vapor transport to central China while water vapor is diverged northward and southward in northern and southern China (Figure S8).

Including the TP's radiation-topography interaction overall improves the *P* simulations in SA and EA. This is already apparent in Figure 2c,d for annual P and Figure 2g,h for summer P, as the differences between TOP_TP and PP_Globe generally have opposite signs compared to the difference between PP_Globe and the benchmark data. More specifically, PP_Globe shows high correlations to the GPCP especially in cold seasons (Table S4) for both SA and EA. PP_Globe overall overestimates annual *P* in SA with the wet mean bias of +0.95 mm/day, while it shows a small positive mean bias of +0.18 mm/day in EA. In summer, PP_Globe has larger overestimations over most SA regions with a mean bias of +2.53 mm/day, and the difference between PP_Globe and GPCP shows heterogeneous spatial distribution in EA (Figure 2g). Specifically, the difference in East China shows a "north wet– middle cold– south wet" tripolar structure in East China. Large positive and negative differences are found in the ocean regions of EA, while the land regions of EA generally show a small deviation from GPCP. By contrast, TOP_TP shows higher R values of 0.66 and 0.83 respectively in summer and autumn than PP_Globe (0.62 and 0.74, respectively) in SA, while TOP_TP has similar R values with PP_Globe across seasons in EA. TOP_TP overall reduces the wet bias in India (Figure 2d,h). Note that the summer spatial patterns between the difference of TOP_TP and PP_Globe and the difference between of PP_Globe and GPCP are opposite in East China (Figure 2g-h), which demonstrates that TOP_TP reduces the summer *P* biases in East China with the tripolar structure.

Although the differences between TOP_Globe and PP_Globe overall show similar patterns to that between TOP_TP and PP_Globe, there are some large differences especially in India (Figure

S11). These demonstrate that the radiation-topography interactions in non-TP regions also affect the climate of the Asian regions.

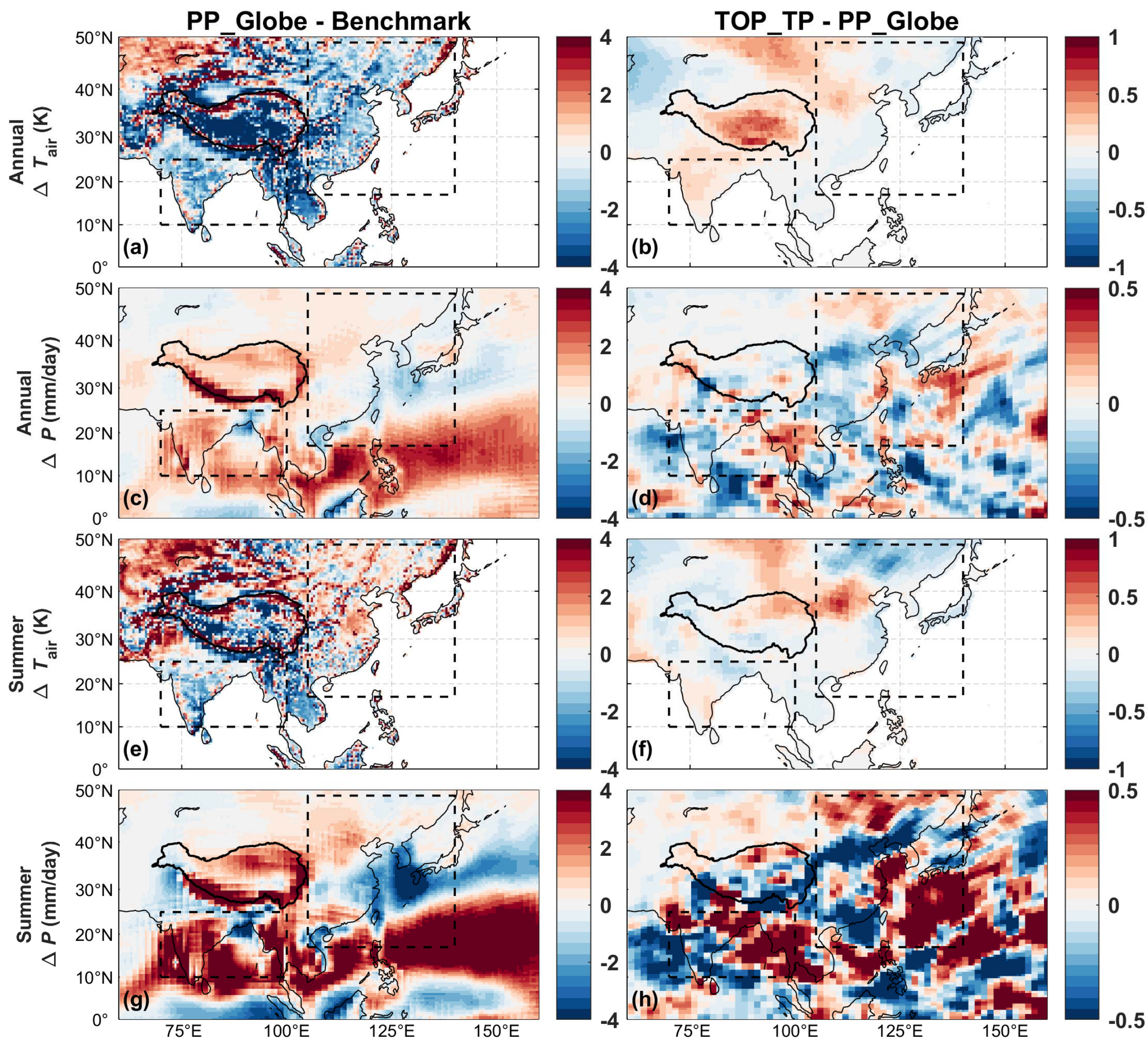

Figure 2. Teleconnected impacts of radiation-topography interaction on annual and summer air temperature (T_{air}) and precipitation (*P*). Panels (a,c,e,f) are the differences between PP_Globe and Benchmark datasets, and Panels (b,d,f,h) are the differences between TOP_TP and PP_Globe. For each panel, the black solid line is the boundary of TP, and the two black dashed lines are the boundaries of South and East Asia regions defined in Section 2.3.

4 Discussion and Conclusions

Radiation-topography interaction plays an important role in regulating regional climate. By using land-atmosphere coupled sensitivity experiments based on E3SM, we demonstrate that radiation-topography interaction can influence the TP's surface energy balance by reducing α and f_{sno} (Figure 1), which is consistent with the offline ELM simulations [*Hao et al.*, 2021]. Such interaction further warms the regional near-surface atmosphere, modifies the clouds and affect the local *P* (Figure 1). Accounting for such interaction in E3SM shows reduced cold biases over the whole TP (Figure 2) especially in winter, which is in line with Lee et al. (2019) and Fan et al. (2019). The interaction between radiation and topography is also expected to affect the glacier evolution over the TP by accelerating glacier melt and retreat [*Kraaijenbrink et al.*, 2017; *Tang et al.*, 2023].

Radiation-topography interaction over the TP could further affect the East and South Asian climate. Due to the important role of TP as an "elevated heat pump", the topography-induced albedo change can affect the wind and moisture transport over SA and EA, and thus redistribute *P* (Figure 2) over the Asian regions [*Tang et al.*, 2023]. Specifically, the TP's albedo change can affect the intensities and movement of the South Asian High and West Pacific Subtropical High [*Tang et al.*, 2023] through the Rossby wave trains [*Wang et al.*, 2008]. Our simulations show that these changes are manifested in the iconic tripolar pattern change in *P* in East China which is a dominant pattern of *P* variability in the region. The land surface temperature anomalies over the TP have significant impacts on the East Asian summer monsoon precipitation [*Diallo et al.*, 2022]. Besides, the snow cover change in winter over the TP is also linked to the variation of summer *P* in the downstream regions of China [*Li et al.*, 2018; *You et al.*, 2020]. All of these can contribute to the change of regional seasonal *P* patterns and timing. However, the nonlinear responses of Asian climate to the topography-induced albedo change and associated dominant pathways need further investigations. It is noted that non-TP mountainous regions can also contribute to the change of *P* patterns in the Asian regions (Figure S11), which needs further analysis.

There are still large systemic biases in simulating surface climate over the TP and surrounding regions, despite improved E3SM model performance against the benchmark datasets after accounting for radiation-topography interaction. Such issues have been found in all the ESMs (including E3SM) participating in the "Impact of Initialized Land Surface Temperature and Snowpack on Subseasonal to Seasonal Prediction" project [*Xue et al.*, 2021]. The large cold and wet biases imply that there are some additional important physical processes over the TP but are not well represented or even missing in E3SM and other ESMs. For example, the coupling of convection to the large-scale environment needs to be improved to reduce the *P* biases in E3SM [*Zheng et al.*, 2019]. The T_{air} and *P* biases in E3SM further contribute to the uncertainties in snowpack simulations [*Brunke et al.*, 2021]. Besides, the LAP deposition over the TP shows large impacts on the TP's snow cover [*Sarangi et al.*, 2020] and Asian monsoon climate [*Qian et al.*, 2011]. However, there is still limited knowledge on the snow grain shape and mixing state between LAP and snow grain over the TP, which has been demonstrated to have large impacts on TP's energy balance and water cycle [*Hao et al.*, 2023; *He et al.*, 2018]. Better considering the snow-aerosol-radiation interaction is necessary to reduce the uncertainties in simulating climate over the TP and surrounding regions.

Our findings underscore the important regional and teleconnected impacts of radiation-topography interaction over the TP. Improved understanding of the topographic roles stresses the significance of parameterizing such important physical processes in CMIP6 models for future climate projections. Neglecting such interaction will bias the simulations and projections of surface energy balance, snow processes and surface climate over complex terrain and surrounding regions.

Acknowledgments

This research was supported by the U.S. Department of Energy (DOE), Office of Science, Office of Biological and Environmental Research, Earth System Model Development program area, as part of the Climate Process Team projects. The reported research was conducted at the Pacific Northwest National Laboratory (PNNL), which is operated for the DOE by the Battelle Memorial Institute under contract DE-AC05-76RL01830. This research used the computational resources of the National Energy Research Scientific Computing Center, and DOE's Biological and Environmental Research Earth System Modeling program's Compy computing cluster located at PNNL.

Open Research

The codes of E3SMv2 are publicly available at https://github.com/E3SM-Project and in this study we used the git commit 8c716b9 of E3SM. Codes and data to reproduce all results and plot all figures are available at https://doi.org/10.5281/zenodo.8327334.

References

Adler, R. F., et al. (2018), The Global Precipitation Climatology Project (GPCP) Monthly Analysis (New Version 2.3) and a Review of 2017 Global Precipitation, *Atmosphere*, *9*(4), 138.

Arnold, N. S., W. G. Rees, A. J. Hodson, and J. Kohler (2006), Topographic controls on the surface energy balance of a high Arctic valley glacier, *Journal of Geophysical Research: Earth Surface*, *111*(F2).

Bair, E. H., T. Stillinger, and J. Dozier (2021), Snow Property Inversion From Remote Sensing (SPIReS): A Generalized Multispectral Unmixing Approach With Examples From MODIS and Landsat 8 OLI, *IEEE Transactions on Geoscience and Remote Sensing*, *59*(9), 7270-7284.

Brunke, M. A., J. Welty, and X. Zeng (2021), Attribution of Snowpack Errors to Simulated Temperature and Precipitation in E3SMv1 Over the Contiguous United States, *Journal of Advances in Modeling Earth Systems*, *13*(10), e2021MS002640.

Burrows, S. M., et al. (2020), The DOE E3SM v1.1 Biogeochemistry Configuration: Description and Simulated Ecosystem-Climate Responses to Historical Changes in Forcing, *Journal of Advances in Modeling Earth Systems*, *12*(9), e2019MS001766.

Cai, S., A. Huang, K. Zhu, W. Guo, Y. Wu, and C. Gu (2023), The Forecast Skill of the Summer Precipitation Over Tibetan Plateau Improved by the Adoption of a 3D Sub-Grid Terrain Solar Radiative Effect Scheme in a Convection-Permitting Model, *Journal of Geophysical Research: Atmospheres*, *128*(11), e2022JD038105.

Comola, F., B. Schaefli, P. D. Ronco, G. Botter, M. Bavay, A. Rinaldo, and M. Lehning (2015), Scale-dependent effects of solar radiation patterns on the snow-dominated hydrologic response, *Geophysical Research Letters*, *42*(10), 3895-3902.

Cui, T., C. Li, and F. Tian (2021), Evaluation of Temperature and Precipitation Simulations in CMIP6 Models Over the Tibetan Plateau, *Earth and Space Science*, *8*(7), e2020EA001620.

Dang, C., C. S. Zender, and M. G. Flanner (2019), Intercomparison and improvement of two-stream shortwave radiative transfer schemes in Earth system models for a unified treatment of cryospheric surfaces, *The Cryosphere*, *13*(9), 2325-2343.

Diallo, I., Y. Xue, Q. Chen, X. Ren, and W. Guo (2022), Effects of spring Tibetan Plateau land temperature anomalies on early summer floods/droughts over the monsoon regions of South East Asia, *Climate Dynamics*.

Dubayah, R., and P. M. Rich (1995), Topographic solar radiation models for GIS, *International Journal of Geographical Information Systems*, *9*(4), 405-419.

Fan, X., Y. Gu, K.-N. Liou, W.-L. Lee, B. Zhao, H. Chen, and D. Lu (2019), Modeling study of the impact of complex terrain on the surface energy and hydrology over the Tibetan Plateau, *Climate Dynamics*, *53*(11), 6919-6932.

Golaz, J.-C., et al. (2022), The DOE E3SM Model Version 2: Overview of the Physical Model and Initial Model Evaluation, *Journal of Advances in Modeling Earth Systems*, *14*(12), e2022MS003156.

Gu, C., A. Huang, Y. Zhang, B. Yang, S. Cai, X. Xu, J. Luo, and Y. Wu (2022), The Wet Bias of RegCM4 Over Tibet Plateau in Summer Reduced by Adopting the 3D Sub-Grid Terrain Solar Radiative Effect Parameterization Scheme, *Journal of Geophysical Research: Atmospheres*, *127*(21), e2022JD037434.

Hao, D., G. Bisht, Y. Gu, W. L. Lee, K. N. Liou, and L. R. Leung (2021), A parameterization of sub-grid topographical effects on solar radiation in the E3SM Land Model (version 1.0): implementation and evaluation over the Tibetan Plateau, *Geosci. Model Dev.*, *14*(10), 6273-6289.

Hao, D., G. Bisht, M. Huang, P.-L. Ma, T. Tesfa, W.-L. Lee, Y. Gu, and L. R. Leung (2022), Impacts of Sub-Grid Topographic Representations on Surface Energy Balance and Boundary Conditions in the E3SM Land Model: A Case Study in Sierra Nevada, *Journal of Advances in Modeling Earth Systems*, *14*(4), e2021MS002862.

Hao, D., et al. (2023), Improving snow albedo modeling in the E3SM land model (version 2.0) and assessing its impacts on snow and surface fluxes over the Tibetan Plateau, *Geosci. Model Dev.*, *16*(1), 75-94.

He, C., M. G. Flanner, F. Chen, M. Barlage, K. N. Liou, S. Kang, J. Ming, and Y. Qian (2018), Black carbon-induced snow albedo reduction over the Tibetan Plateau: uncertainties from snow grain shape and aerosol–snow mixing state based on an updated SNICAR model, *Atmos. Chem. Phys.*, *18*(15), 11507-11527.

Huffman, G. J., R. F. Adler, P. Arkin, A. Chang, R. Ferraro, A. Gruber, J. Janowiak, A. McNab, B. Rudolf, and U. Schneider (1997), The Global Precipitation Climatology Project (GPCP) Combined Precipitation Dataset, *Bulletin of the American Meteorological Society*, *78*(1), 5-20.

Jung, M., S. Koirala, U. Weber, K. Ichii, F. Gans, G. Camps-Valls, D. Papale, C. Schwalm, G. Tramontana, and M. Reichstein (2019), The FLUXCOM ensemble of global land-atmosphere energy fluxes, *Scientific Data*, *6*(1), 74.

Kraaijenbrink, P. D. A., M. F. P. Bierkens, A. F. Lutz, and W. W. Immerzeel (2017), Impact of a global temperature rise of 1.5 degrees Celsius on Asia's glaciers, *Nature*, *549*(7671), 257-260.

Lee, W.-L., K. N. Liou, and A. Hall (2011), Parameterization of solar fluxes over mountain surfaces for application to climate models, *Journal of Geophysical Research: Atmospheres*, *116*(D1).

Lee, W.-L., K.-N. Liou, C.-c. Wang, Y. Gu, H.-H. Hsu, and J.-L. F. Li (2019), Impact of 3-D Radiation-Topography Interactions on Surface Temperature and Energy Budget Over the Tibetan Plateau in Winter, *Journal of Geophysical Research: Atmospheres*, *124*(3), 1537-1549.

Leung, L. R., D. C. Bader, M. A. Taylor, and R. B. McCoy (2020), An Introduction to the E3SM Special Collection: Goals, Science Drivers, Development, and Analysis, *Journal of Advances in Modeling Earth Systems*, *12*(11), e2019MS001821.

Li, W., W. Guo, B. Qiu, Y. Xue, P.-C. Hsu, and J. Wei (2018), Influence of Tibetan Plateau snow cover on East Asian atmospheric circulation at medium-range time scales, *Nature Communications*, *9*(1), 4243.

Liou, K. N., Y. Gu, L. R. Leung, W. L. Lee, and R. G. Fovell (2013), A WRF simulation of the impact of 3-D radiative transfer on surface hydrology over the Rocky Mountains and Sierra Nevada, *Atmos. Chem. Phys.*, *13*(23), 11709-11721.

Nasa/Larc/Sd/Asdc (2023), CERES Energy Balanced and Filled (EBAF) TOA and Surface Monthly means data in netCDF Edition 4.2, edited.

Olson, M., and S. Rupper (2019), Impacts of topographic shading on direct solar radiation for valley glaciers in complex topography, *The Cryosphere*, *13*(1), 29-40.

Proy, C., D. Tanré, and P. Y. Deschamps (1989), Evaluation of topographic effects in remotely sensed data, *Remote Sensing of Environment*, *30*(1), 21-32.

Qian, Y., M. G. Flanner, L. R. Leung, and W. Wang (2011), Sensitivity studies on the impacts of Tibetan Plateau snowpack pollution on the Asian hydrological cycle and monsoon climate, *Atmos. Chem. Phys.*, *11*(5), 1929-1948.

Rittger, K., M. S. Raleigh, J. Dozier, A. F. Hill, J. A. Lutz, and T. H. Painter (2020), Canopy Adjustment and Improved Cloud Detection for Remotely Sensed Snow Cover Mapping, *Water Resources Research*, *56*(6), e2019WR024914.

Sarangi, C., Y. Qian, K. Rittger, L. Ruby Leung, D. Chand, K. J. Bormann, and T. H. Painter (2020), Dust dominates high-altitude snow darkening and melt over high-mountain Asia, *Nature Climate Change*, *10*(11), 1045-1051.

Sirguey, P. (2009), Simple correction of multiple reflection effects in rugged terrain, *International Journal of Remote Sensing*, *30*(4), 1075-1081.

Tang, S., et al. (2023), Regional and tele-connected impacts of the Tibetan Plateau surface darkening, *Nature Communications*, *14*(1), 32.

Thackeray, C. W., and C. G. Fletcher (2016), Snow albedo feedback:Current knowledge, importance, outstanding issues and future directions, *Progress in Physical Geography: Earth and Environment*, *40*(3), 392-408.

Wang, B., Q. Bao, B. Hoskins, G. Wu, and Y. Liu (2008), Tibetan Plateau warming and precipitation changes in East Asia, *Geophysical Research Letters*, *35*(14).
Willmott, C. J., and K. Matsuura (1995), Smart Interpolation of Annually Averaged Air Temperature in the United States, *Journal of Applied Meteorology and Climatology*, *34*(12), 2577-2586.
Wu, G., A. Duan, Y. Liu, J. Mao, R. Ren, Q. Bao, B. He, B. Liu, and W. Hu (2014), Tibetan Plateau climate dynamics: recent research progress and outlook, *National Science Review*, *2*(1), 100-116.
Wu, G., Y. Liu, Q. Zhang, A. Duan, T. Wang, R. Wan, X. Liu, W. Li, Z. Wang, and X. Liang (2007), The Influence of Mechanical and Thermal Forcing by the Tibetan Plateau on Asian Climate, *Journal of Hydrometeorology*, *8*(4), 770-789.
Xue, D., J. Lu, L. R. Leung, H. Teng, F. Song, T. Zhou, and Y. Zhang (2023), Robust projection of East Asian summer monsoon rainfall based on dynamical modes of variability, *Nature Communications*, *14*(1), 3856.
Xue, Y., et al. (2022), Spring Land Temperature in Tibetan Plateau and Global-Scale Summer Precipitation: Initialization and Improved Prediction, *Bulletin of the American Meteorological Society*, *103*(12), E2756-E2767.
Xue, Y., et al. (2021), Impact of Initialized Land Surface Temperature and Snowpack on Subseasonal to Seasonal Prediction Project, Phase I (LS4P-I): organization and experimental design, *Geosci. Model Dev.*, *14*(7), 4465-4494.
Yang, H., X. Shen, J. Yao, and Q. Wen (2020), Portraying the Impact of the Tibetan Plateau on Global Climate, *Journal of Climate*, *33*(9), 3565-3583.
You, Q., T. Wu, L. Shen, N. Pepin, L. Zhang, Z. Jiang, Z. Wu, S. Kang, and A. AghaKouchak (2020), Review of snow cover variation over the Tibetan Plateau and its influence on the broad climate system, *Earth-Science Reviews*, *201*, 103043.
Zhang, X., A. Huang, Y. Dai, W. Li, C. Gu, H. Yuan, N. Wei, Y. Zhang, B. Qiu, and S. Cai (2022), Influences of 3D Sub-Grid Terrain Radiative Effect on the Performance of CoLM Over Heihe River Basin, Tibetan Plateau, *Journal of Advances in Modeling Earth Systems*, *14*(1), e2021MS002654.
Zheng, X., J.-C. Golaz, S. Xie, Q. Tang, W. Lin, M. Zhang, H.-Y. Ma, and E. L. Roesler (2019), The Summertime Precipitation Bias in E3SM Atmosphere Model Version 1 over the Central United States, *Journal of Geophysical Research: Atmospheres*, *124*(16), 8935-8952.
Zhu, Y.-Y., and S. Yang (2020), Evaluation of CMIP6 for historical temperature and precipitation over the Tibetan Plateau and its comparison with CMIP5, *Advances in Climate Change Research*, *11*(3), 239-251.
Zorzetto, E., S. Malyshev, N. Chaney, D. Paynter, R. Menzel, and E. Shevliakova (2023), Effects of complex terrain on the shortwave radiative balance: a sub-grid-scale parameterization for the GFDL Earth System Model version 4.1, *Geosci. Model Dev.*, *16*(7), 1937-1960.